ADVANCED FUNCTIONAL MATERIALS
www.afm-journal.de

A Salt-in-Metal Anode: Stabilizing the Solid Electrolyte Interphase to Enable Prolonged Battery Cycling

*Lin Fu, Xiancheng Wang, Li Wang, Mintao Wan, Yuanjian Li, Zhao Cai, Yuchen Tan, Guocheng Li, Renming Zhan, Zhi Wei Seh, and Yongming Sun**

Metallic lithium (Li) is the ultimate anode candidate for high-energy-density rechargeable batteries. However, its practical application is hindered by serious problems, including uncontrolled dendritic Li growth and undesired side reactions. In this study a concept of "salt-in-metal" is proposed, and a Li/$LiNO_3$ composite foil is constructed such that a classic electrolyte additive, $LiNO_3$, is embedded successfully into the bulk structure of metallic Li by a facile mechanical kneading approach. The $LiNO_3$ reacts with metallic Li to generate Li^+ conductive species (e.g., Li_3N and LiN_xO_y) over the entire electrode. These derivatives afford a stable solid electrolyte interphase (SEI) and effectively regulate the uniformity of the nucleation/growth of Li on initial plating, featuring a low nucleation energy barrier and large crystalline size without mossy morphology. Importantly, these derivatives combined with $LiNO_3$ can in-situ repair the damaged SEI from the large volume change during Li plating/stripping, enabling a stable electrode-electrolyte interface and suppressing side reactions between metallic Li and electrolyte. Stable cycling with a high capacity retention of 93.1% after 100 cycles is obtained for full cells consisting of high-loading $LiCoO_2$ cathode (≈20 mg cm^{-2}) and composite metallic Li anode with 25 wt% $LiNO_3$ under a lean electrolyte condition (≈12 µL) at 0.5 C.

1. Introduction

Metallic Li possesses the highest theoretical specific capacity (3860 mA h g^{-1}) and lowest electrochemical potential (−3.04 V versus standard hydrogen electrode) among anodes, and is the ultimate anode choice for rechargeable batteries.[1,2] To meet the ever-increasing energy demand in various fields, such as electric vehicles, grid storage and portable electronics, metallic Li anode have been widely studied to achieve high energy density Li metal batteries (LMBs).[3,4] However, its practical application is still impeded by several serious issues including uncontrolled Li plating/stripping behavior and undesired side reactions at the anode side due to large volume change and high reactivity of metallic Li during the stripping/plating cycling.[5]

The infinite relative volume change and sluggish Li diffusion kinetics lead to the absence of spatial control of Li plating and can even cause the formation of dangerous dendrites.[6] Metallic Li decomposes salts and solvents in liquid electrolytes, producing a solid electrolyte interphase (SEI) film on its surface.[7] Such SEI film continuously crumbles and repairs due to the large volume change during Li stripping/plating cycling, which continuously consumes active Li and liquid electrolyte and leads to a thick SEI layer.[8,9] The above processes together cause the formation of a loose structure after many cycles and even the pulverization of metallic Li electrode.[10] The situation is severely aggravated under practical battery conditions with high areal capacity loading.[10] Metallic Li in the loose structure of electrode surrounded by thick SEI would be isolated from the surroundings, losing electronic and ionic connection and forming "dead Li", which cannot participate the subsequent electrochemical cycling.[11] The above detrimental processes eventually lead to fast failure of Li metal batteries. More seriously, metallic Li dendrites produced during cycling may penetrate the separator and cause internal short circuit and even safety hazards.[12] Therefore, the design of Li metal electrode with uniform SEI and stable stripping/plating behavior is of vital importance for practical LMBs.

Till now, numerous strategies have been explored to improve Li metal electrodes, including surface protection layer, 3D host, solid electrolyte, and electrolyte engineering.[13–16] Among the various strategies, using electrolyte additives is considered as one of the most facile and effective approaches.[17] Additives in electrolyte can effectively regulate metallic Li deposition by the optimization of the solvation structures of Li^+ and the reinforcement of physical and chemical properties of SEI.[17,18]

L. Fu, X. Wang, M. Wan, Y. Li, Z. Cai, Y. Tan, G. Li, R. Zhan, Prof. Y. Sun
Wuhan National Laboratory for Optoelectronics
Huazhong University of Science and Technology
Wuhan 430074, China
E-mail: yongmingsun@hust.edu.cn
Prof. L. Wang
Institute of Nuclear and New Energy Technology
Tsinghua University
Beijing 100084, China
Prof. Z. W. Seh
Institute of Materials Research and Engineering
Agency for Science, Technology and Research (A*STAR)
Singapore 138634, Singapore

The ORCID identification number(s) for the author(s) of this article can be found under https://doi.org/10.1002/adfm.202010602.

DOI: 10.1002/adfm.202010602

Consequently, the nucleation of metallic Li can be altered, the growth of dendritic Li can be suppressed/eliminated, and the side reactions between metallic Li and electrolyte can be hindered.[19] Among various additives, $LiNO_3$ is highly effective in stabilizing the Li metal anode by regulating the uniformity and ionic conductivity of SEI.[20,21] With the reduction of $LiNO_3$ to form rich Li_3N and LiN_xO_y species uniformly distributed in the SEI film, Li^+ diffusion is promoted and Li plating/stripping behavior is regulated.[22,23] However, the extremely low solubility of $LiNO_3$ in the mostly widely used carbonate electrolyte (≈800 ppm) is a huge barrier for practical application, since the tiny amount of $LiNO_3$ in electrolyte would be exhausted quickly over cycling.[24,25] Therefore, one big challenge for using $LiNO_3$ additive is to find a sustainable way to avoid its rapid depletion and achieve long-term effect of $LiNO_3$ on cycling. To overcome this problem, several effective strategies have been explored, including utilizing solubilizers to enhance the solubility of $LiNO_3$ in carbonate electrolyte, and using an interfacial layer with excess solid $LiNO_3$ between the electrode and separator which can release during the electrochemical cycling.[22–25] Despite these great achievements, new facile strategies for introducing electrolyte additive ($LiNO_3$) remain to be developed to solve the inherent problem of Li metal and realize practical battery application.

Herein, we propose a novel design to afford a stable SEI by direct introduction of $LiNO_3$ into metallic Li foil electrode in response to the challenge of low solubility in carbonate electrolyte. Modest doses of $LiNO_3$ in the composite electrode can avoid its fast exhaustion and afford a long-term effect on cycling. A $Li/LiNO_3$ (LLNO) composite foil is designed and fabricated by multiple cold rolling operations of $LiNO_3$ powders and metallic Li. Metallic Li is soft and sticky, which helps to form uniform composite of the two components and maintain foil structure of the LLNO composite during the operation. $LiNO_3$ can be reduced by metallic Li according to the following equations:[26]

$$LiNO_3 + 2Li \rightarrow LiNO_2 + Li_2O \quad \Delta H_{\text{calculated}} = -406 \text{ kJ mol}^{-1} \tag{1}$$

$$LiNO_2 + 6Li \rightarrow Li_3N + 2Li_2O \quad \Delta H_{\text{calculated}} = -857 \text{ kJ mol}^{-1} \tag{2}$$

These reaction products participate in the formation of SEI, which regulate the electrochemical behavior of metallic Li and realize dendrite-free Li plating with large particle size in the routine carbonate electrolyte (1 м $LiPF_6$ in EC/DMC/EMC). On the other hand, the reaction products that are buried in the bulk of metallic Li can enhance Li^+ diffusion within the entire foil electrode, which help to eliminate the dendrite growth of metallic Li. The dense plating of metallic Li with large particles and small accessible surface area to liquid electrolyte suppresses the side reactions between metallic Li and electrolyte, reduces the consumption of liquid electrolyte and active Li, and avoids the formation of highly porous electrode structure and its further pulverization. Note that the cracks and reconstructions of SEI are hard to be avoided and the initial SEI would not be maintained during cycling due to the large volume change and high reactivity of metallic Li, and $LiNO_3$ and its derivatives are continuously consumed over long-term cycling. In our LLNO composite electrode, modest doses of $LiNO_3$ and its derivatives in the electrode enables stable SEI, by participating in the effective repair of the initial SEI or the formation of new SEI, which enables prolonged cycle life. With 25 wt% $LiNO_3$ in the LLNO composite electrode (LLNO-25), symmetric cell exhibits stable cycling over 600 hours at 1 mA cm^{-2} and 1 mA h cm^{-2} with a low overpotential (45 mV), in contrast to the fast increase in overpotential on cycling and failure within 200 h for the counterpart with pure Li electrode. When coupled commercial $LiCoO_2$ cathode with high active material loading (≈20 mg cm^{-2}), full cell with LLNO-25 composite anode under a lean electrolyte condition (≈12 µL) displays stable cycling with a high capacity retention of 93.1% after 100 cycles at 0.5 C (1 C = 140 mA g^{-1}), while the counterpart with pure Li anode failed after 37 cycles under the same test condition. This work not only presents a new strategy for the introduction of SEI stabilizer with low solubility in electrolyte solvents, but also extends the consequent protective structure from the surface to the bulk of metallic Li electrode, enhancing its electrochemical performance.

2. Results and Discussion

LLNO composite is fabricated through a repeated mechanical rolling/folding operation (namely “mechanical kneading” approach here, **Figure 1**a). During the fabrication, $LiNO_3$ powders were first spread uniformly between two metallic Li foils, forming a $Li|LiNO_3|Li$ sandwich. $LiNO_3$ is then embedded in the soft and sticky metallic Li to form an integrated structure after the first mechanical rolling. The mechanical kneading operation leads to the close contact between $LiNO_3$ and metallic Li. $LiNO_3$ is gradually reduced by metallic Li at their surface during the fabrication of LLNO, generating Li_3N, LiN_xO_y and Li_2O (detailed characterization will be presented later). Such a process also leads to the pulverization of the initial $LiNO_3$ particles accompanied by their reduction with metallic Li, as well as their successful embedment in the metallic Li matrix. Thus, a LLNO composite with good dispersion of $LiNO_3$ and its derivatives within the entire foil electrode is achieved after the mechanical kneading operation. The SEI on the pure Li anode surface breaks and re-forms during the Li stripping/plating cycle, leading to the formation of thick SEI and even “dead Li” (Figure 1b). The $LiNO_3$ derivatives on the surface of the composite electrode will participate the formation of SEI film (namely $Li_3N/LiN_xO_y/Li_2O$-rich SEI) during electrochemical cycling. This $Li_3N/LiN_xO_y/Li_2O$-rich SEI can alter the nucleation/growth of metallic Li, resulting in the uniform plating of Li without the formation of dendritic morphology. The uniform plating of metallic Li with low accessible surface area exposed to liquid electrolyte reduces the overall amount of SEI and significantly suppresses the formation of “dead Li” (Figure 1c and Figure S1, Supporting Information). The uniform dispersion of $LiNO_3$ and its derivatives in the bulk of the LLNO composite during cycling avoids the exhaustion of $LiNO_3$ in the electrolyte during cycling and helps to make a stable SEI and enable long cycle life of batteries. Moreover, the Li^+ conductive species of $LiNO_3$ derivatives in the bulk of the LLNO composite can enhance the Li^+ diffusion over the entire electrode. The direct introduction of $LiNO_3$ into metallic Li electrode provides a fresh

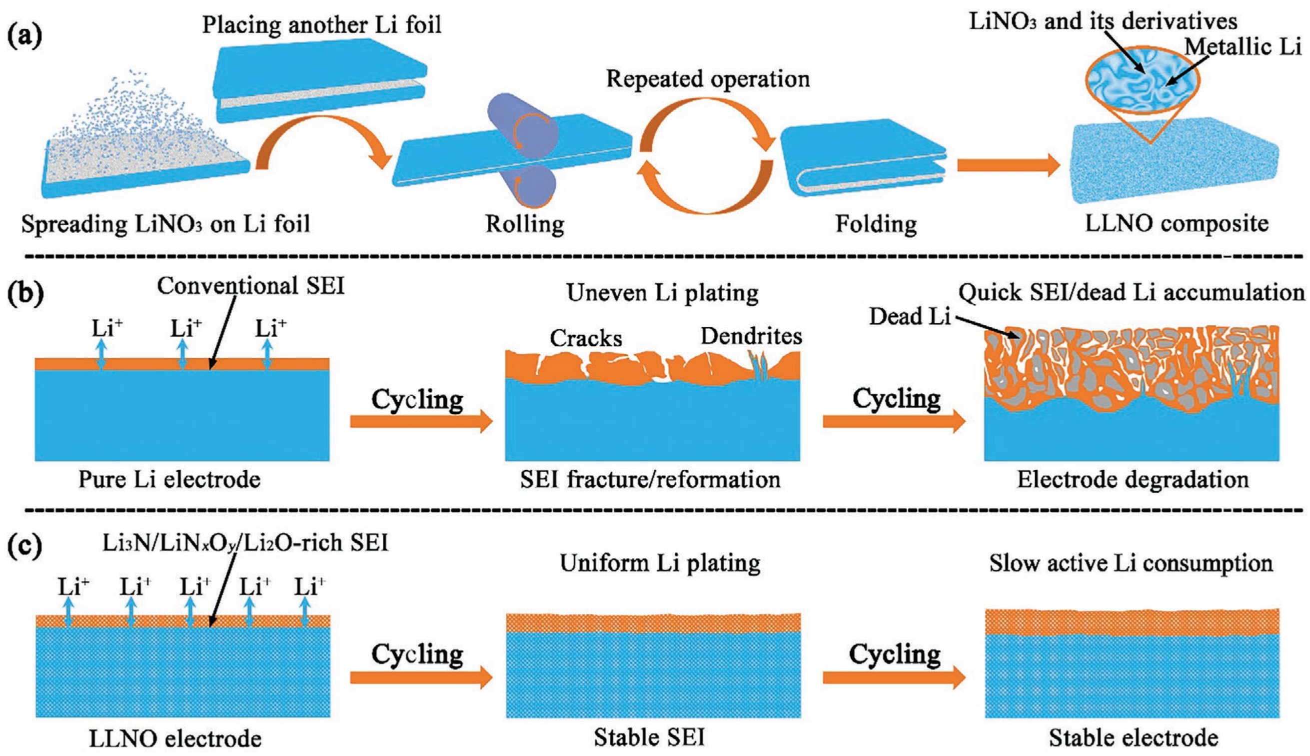

Figure 1. a) The fabrication of LLNO composite. The evolution of b) pure Li and c) LLNO composite electrodes during electrochemical cycling. The $Li_3N/LiN_xO_y/Li_2O$-rich SEI of the LLNO composite electrode enables fast migration of Li^+ through the SEI, uniform Li plating behavior, and prolonged cycle life.

and facile design for achieving stable metallic Li anode in carbonate electrolyte, which is beneficial for mass production to meet practical applications.

LLNO composites with different contents (x wt%) of the initial $LiNO_3$ were fabricated and their electrochemical property was investigated using symmetric cell configuration at 1 mA cm^{-2} and 1 mA h cm^{-2} (x = 5, 10, 15, 20, 25, or 30). It is worth noting here that nucleation of metallic Li is closely related to the consequent plating behavior of Li.[27] As shown in **Figure 2**a and Table S1, Supporting Information, the initial nucleation overpotential decreases gradually with the increase of $LiNO_3$ probably due to the change of microstructure and composition of SEI after the introduction of $LiNO_3$. The $LiNO_3$ derivatives, including LiN_xO_y and Li_3N etc, are able to change the plating behavior of metallic Li by regulating the uniformity and ionic conductivity of SEI.[20,21] Also, the cycling stability of LLNO composite is improved gradually with the increase of $LiNO_3$ content and the LLNO composite containing 25 wt% $LiNO_3$ (LLNO-25) exhibits the best cycling stability among all the samples (Figure 2b and Figures S2–S6, Supporting Information). Stable cycling with constant voltage profiles for the LLZO-25 composite electrode is achieved for 600 hours with a low average overpotential of ≈45 mV, while significant increase in overpotential is observed for the pure Li electrode and it reaches ≈130 mV after 300 h cycling (Figure 2b). Therefore, the LLNO-25 composite is chosen for further study and it displays a high specific capacity of ≈2423.3 mA h g^{-1} (Figure S7, Supporting Information). When the test current density and area capacity are fixed at 3 mA cm^{-2} and 3 mA h cm^{-2}, stable voltage profiles were observed for the symmetric LLNO-25||LLNO-25 cell during more than 200 h cycling, while fast increase in overpotential was observed for the symmetric Li||Li cell after 60 h cycling (Figure S8, Supporting Information). The reduced overpotential for the nucleation and plating of metallic Li and the enhanced cycling stability may arise from the as-formed stable SEI that possesses high ionic conductivity and regulates the electrochemical plating/stripping behavior of metallic Li.[28,29]

X-ray diffraction (XRD) was employed to investigate the phase information of the LLNO-25 composite. Diffraction peaks for $LiNO_3$ (JCPDS#80-0203) and metallic Li (JCPDS#89-3940) were observed in the XRD patterns for the LLNO-25 composite, suggesting the successful composite of $LiNO_3$ and metallic Li (Figure 2c and Figure S9, Supporting Information). After storage in Ar atmosphere for two weeks, no new peaks were observed, indicating the good stability of the LLNO-25 composite (Figure 2c and Figure S10, Supporting Information). It is noted that phase information about $LiNO_3$ derivatives such as LiN_xO_y and Li_3N did not appear in the XRD pattern of the LLNO-25 composite, indicating their ultrafine crystalline size or amorphous structure. X-ray photoelectron spectroscopy (XPS) was used to further detect the elemental composition and chemical state of LLNO-25 composite. Figure 2d displays the high-resolution XPS spectrum of N 1s for the LLNO-25 composite. A strongest peak at 404.2 eV is observed, which corresponds to $LiNO_2$.[23,30] Two weak peaks at 401.2 and 398.2 eV are shown, which are related to the characteristic signals of LiN_xO_y and Li_3N, respectively.[24,30,31] A moderate peak located at 407.8 eV can be indexed to $LiNO_3$.[32] Moreover, the existence

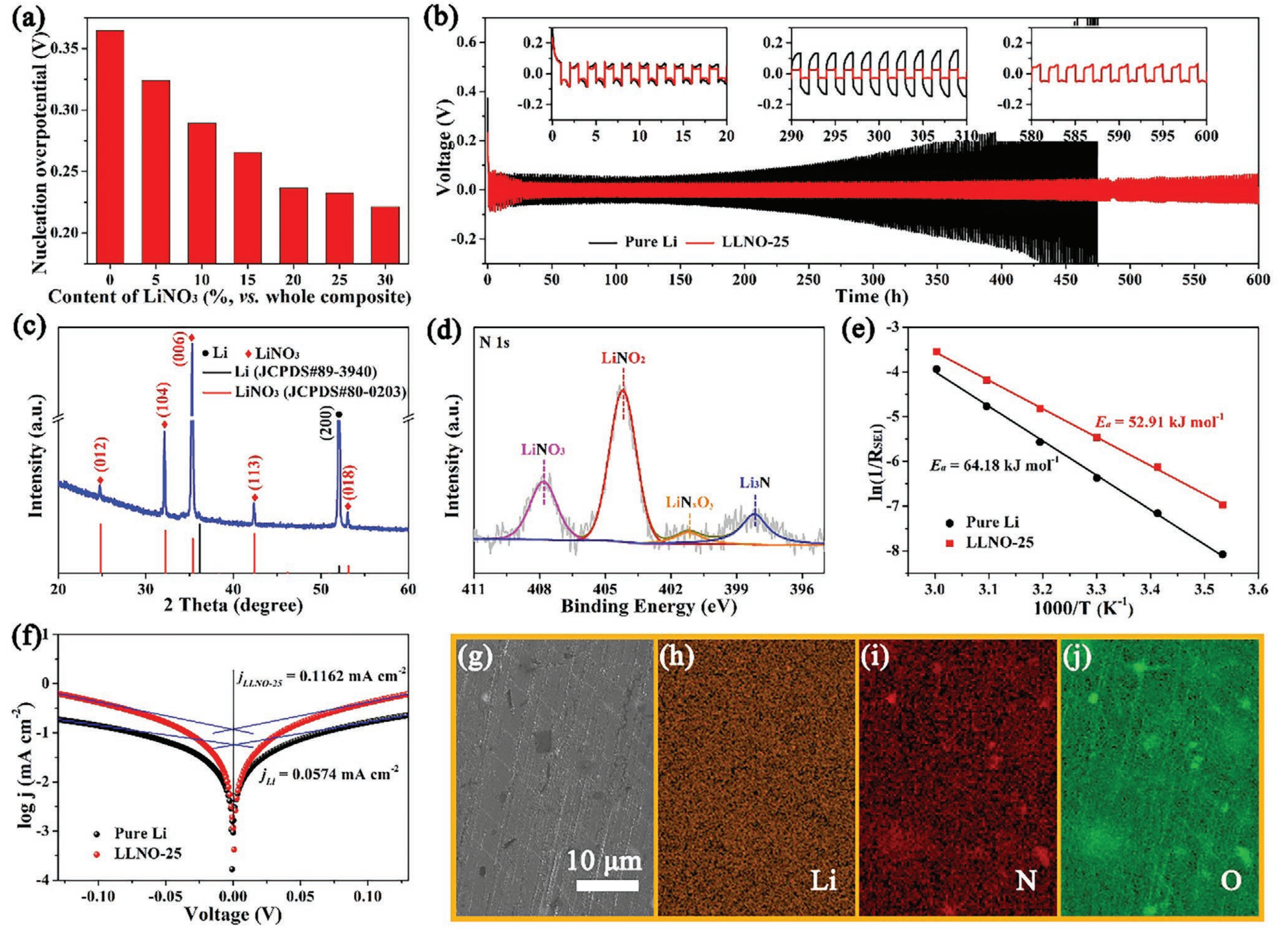

Figure 2. a) Nucleation overpotential during the initial Li plating, which obtained from the symmetric cells with LLNO electrodes with different contents of $LiNO_3$ at 1 mA cm^{-2} and 1 mA h cm^{-2}. b) Galvanostatic voltage profiles of Li||Li and LLNO-25||LLNO-25 symmetric cells at 1 mA cm^{-2} and 1 mA h cm^{-2}. c) XRD pattern of the LLNO-25 composite. d) High-resolution N 1s XPS spectrum of the LLNO-25 composite. e) Activation energies of Li^+ through the SEI film for pure Li and LLNO-25 composite electrodes. The results were derived from Nyquist plots and Arrhenius equation. f) Tafel curves of the Li||Li and LLNO-25||LLNO-25 symmetric cells derived from linear sweep voltammetry (LSV) tests. g) Top-view SEM image of the LLNO-25 composite and h–j) the corresponding EDS mapping images.

of $LiNO_2$, LiN_xO_y, and Li_3N are verified by the results of high-resolution Li 1s and O 1s XPS spectra (Figure S12, Supporting Information).[22–24,30,31] Therefore, certain amount of $LiNO_3$ is reduced to LiN_xO_y and Li_3N by metallic Li during the mechanical kneading operation. The formation of these Li conductive species and their distribution in the LLNO composite can enable fast Li^+ diffusion on the surface and bulk of the entire electrode, which leads to easy nucleation and uniform plating of metallic Li.[22,33] The plating of metallic Li must overcome the energy barrier for the migration of Li^+ across the SEI film. According to the previous studies, the apparent activation energy of Li^+ migration across the SEI film (E_a) can be obtained by the electrochemical impedance spectroscopy (EIS) measurements of symmetrical cells with pure Li and LLNO-25 composite electrodes under different temperatures (Figure S13a,b, Supporting Information).[34] A suitable equivalent circuit was established (Figure S13c, Supporting Information) to analyze the as-measured EIS curves from 283 to 333 K and to obtain the resistance value of Li^+ through the SEI film (R_{SEI}, Figure S13d, Supporting Information). According to the Arrhenius equation:[34,35]

$$\frac{T}{R_{SEI}} = Ae^{-\frac{E_a}{RT}} \tag{3}$$

where T, A, and R are the absolute temperature in kelvin, pre-exponential factor, and standard gas constant, respectively. As shown in Figure 2e, the E_a of the LLNO-25 composite (52.91 kJ mol^{-1}) is much lower than that of the pure Li (64.18 kJ mol^{-1}), which indicates that the introduction of $LiNO_3$ reduces the activation energy of Li^+ diffusion through the SEI of the composite electrode. Such advantage arises from the enhanced ionic conductivity of SEI due to presence of $LiNO_3$ derivatives. Importantly, improving Li^+ conductivity of SEI can enlarge the grain size of Li deposits,[25] which helps to suppress the formation of dendritic Li, reduce the depletion of active Li and prevent the fast accumulation of "dead Li" during cycling. The exchange current density (j_0) derived from the Tafel plots is applied to further verify the advantage for introducing $LiNO_3$ into the bulk of metallic Li. As shown in Figure 2f, the value of exchange current density of the LNNO-25 is two times higher than that of the pure Li (0.1162 mA cm^{-2} for the LNNO-25 vs 0.0574 mA cm^{-2} for the pure Li), indicating much better charge transfer capability at the Li electrode/electrolyte interface for the LLNO-25 electrode resulting from its highly conductive SEI.[36–38] Importantly, the rapid charge transfer at the interface of Li electrode and electrolyte can restrain the uneven Li plating and improve the electrochemical reaction kinetics.[25,29,34,37,39] LLNO-25 composite foil displays same luster (Figure S14, Supporting Information) and surface morphology as pure metallic Li foil (Figure S15, Supporting Information). Scanning electronic microscopy (SEM) image (Figure 2g) and corresponding energy dispersive X-ray spectroscopy (EDS) mapping images of the LLNO-25 composite (Figure 2h–j) demonstrate the uniform distribution of elements of Li, N, and O in the LLNO-25 composite in the measured area except tiny amount of particles with much reduced size (1 μm or less) in contrast to the initial $LiNO_3$ particles in the size of tens of micrometers (Figure S16, Supporting Information), indicating that $LiNO_3$ and its derivatives are successfully embedded into the matrix of metallic Li by mechanical kneading operation. In addition, $LiNO_3$ particles with large size (Figure S16, Supporting Information) are not observed in above results, suggesting the pulverization/crushing of the $LiNO_3$ particles during its continuous reaction with metallic Li and the mechanical rolling process, which is an important factor in realizing a uniform composite.

The presence of $LiNO_3$ in the electrolyte can avoid the rapid failure of metallic Li electrode by altering the composition, structure and properties of SEI, and consequently regulating Li deposition.[24,40] To reveal the effect of $LiNO_3$ in the as-designed LLNO electrode, SEM was employed to investigate the morphology of the cycled LLZO-25 and pure Li foil electrodes in symmetric cell configuration. Figure S17a, Supporting Information shows a top-view SEM image of the pure Li electrode after the initial Li stripping at 1 mA cm^{-2} and 1 mA h cm^{-2}. Large and irregular cavities were randomly distributed on the surface of the electrode and the depth of the cavities could reach several tens of microns, suggesting inhomogeneous electrochemical Li stripping behavior (Figure S17a, Supporting Information). In contrast, the LLNO-25 electrode exhibits a relatively uniform electrochemical Li stripping behavior. Shallow and broad cavities were observed on the surface of the LLNO-25 electrode after Li stripping (Figure S17b, Supporting Information). The different Li stripping behaviors of the LLNO-25 and pure Li metal electrodes arise from the effect of $LiNO_3$ in the LLNO-25 electrode, which regulates the uniformity and improves the ionic conductivity of SEI.[22,33] Moreover, the relatively smooth surface of the LLNO-25 electrode can adjust the Li^+ flux and further enable uniform Li deposition. Figure S17c–f, Supporting Information shows selected-area EDS mapping images of the LLNO-25 electrode after Li stripping. The results indicate that $LiNO_3$ and its derivatives are evenly distributed in the electrode after Li stripping, suggesting their good stability during electrochemical cycling. Whisker-like Li deposits were observed for the pure Li electrode after initial Li plating, the diameters of which are less than 0.2 μm (Figure S18a, Supporting Information). In contrast, the LLNO-25 electrode displays granular microstructure with grain size up to 10 μm (Figure S18b, Supporting Information), which could eliminate the risk of internal short circuit caused by growth of Li dendrite and enable stable electrochemical cycling with high Columbic efficiency. After ten Li stripping/plating cycles, the LLNO-25 electrode presents a smooth surface with compactly arranged spherical metallic Li deposits (**Figure 3**a and Figure S19a, Supporting Information), while the pure Li electrode shows loose accumulation of metallic Li whiskers (Figure 3d and Figure S19c, Supporting Information). The significant change in the morphology for the cycled LLNO-25 and pure Li electrodes arises from the improved SEI for the LLNO-25 electrode due to the involvement of the $LiNO_3$ and its derivatives from the bulk of the electrode, which enables a stable SEI for long-term cycling. Dense metallic Li microstructure was also observed for the LLNO-25 electrode after 50 Li plating/stripping cycles, verifying the ability of the enhanced SEI in regulating the Li plating/stripping (Figure 3b and Figure S19b, Supporting Information). In contrast, the pure Li electrode exhibits a loose and dendrite-containing surface structure entangled with thick SEI. Meanwhile, large cracks in several micrometers are observed on the surface of the cycled pure Li electrode (Figure 3e and Figure S19d, Supporting Information). The metallic Li layer involved in the stripping/plating cycling is densely packed and the thickness for the reaction layer, referring to the specific layer that participates in the electrochemical stripping/plating reaction, is only ≈50 μm for the LLNO-25 after 50 cycles (Figure 3c), while this reaction layer reaches ≈100 μm for the pure metallic Li electrode (Figure 3f). For pure metallic Li electrode, the generated mossy Li with high surface area continuously reacts with electrolyte over cycling, and leads to the fast consumption of liquid electrolyte and active Li, and the accumulation of highly resistive SEI.[9] Such a process also results the fast formation of "dead Li", which are buried with highly resistive SEI and would not participate in the following electrochemical reactions, since its electrical connection is cut off by thick SEI. Due to the relatively low utilization of metallic Li in the loose surface layer, bulk Li under such layer has to participate in the subsequent electrochemical cycling, which makes the loose layer continuously grow towards the bulk Li over cycling. This phenomenon will dramatically increase the battery impedance and directly lead to failure of batteries. The dense structure of the surface layer of the LLNO-25 electrode are direct evidence of the uniformity of SEI. Therefore, the introduction of $LiNO_3$ in the bulk Li helps to form a stable SEI and enable reversible metallic Li plating/stripping behavior. These results suggest the significant effect of the "$LiNO_3$-in-Li" structure in regulating the electrochemical Li plating/stripping behavior of metallic Li.

The accumulation of SEI leads to increase in battery impedance, and final battery degradation and failure. EIS measurement was conducted for the symmetric cells after various cycles (after 50, 100, and 150 cycles) to verify the ability of LLNO-25 electrode in suppressing the side reactions and improving the electrochemical performance. The Nyquist plots of symmetric LLNO-25||LLNO-25 and Li||Li cells are provided in Figure 3g,h, respectively, and the values of each resistance component were extracted using a suitable equivalent circuit model (inset of Figure 3g). The value of each resistance component of the LLNO-25 electrode is much smaller than

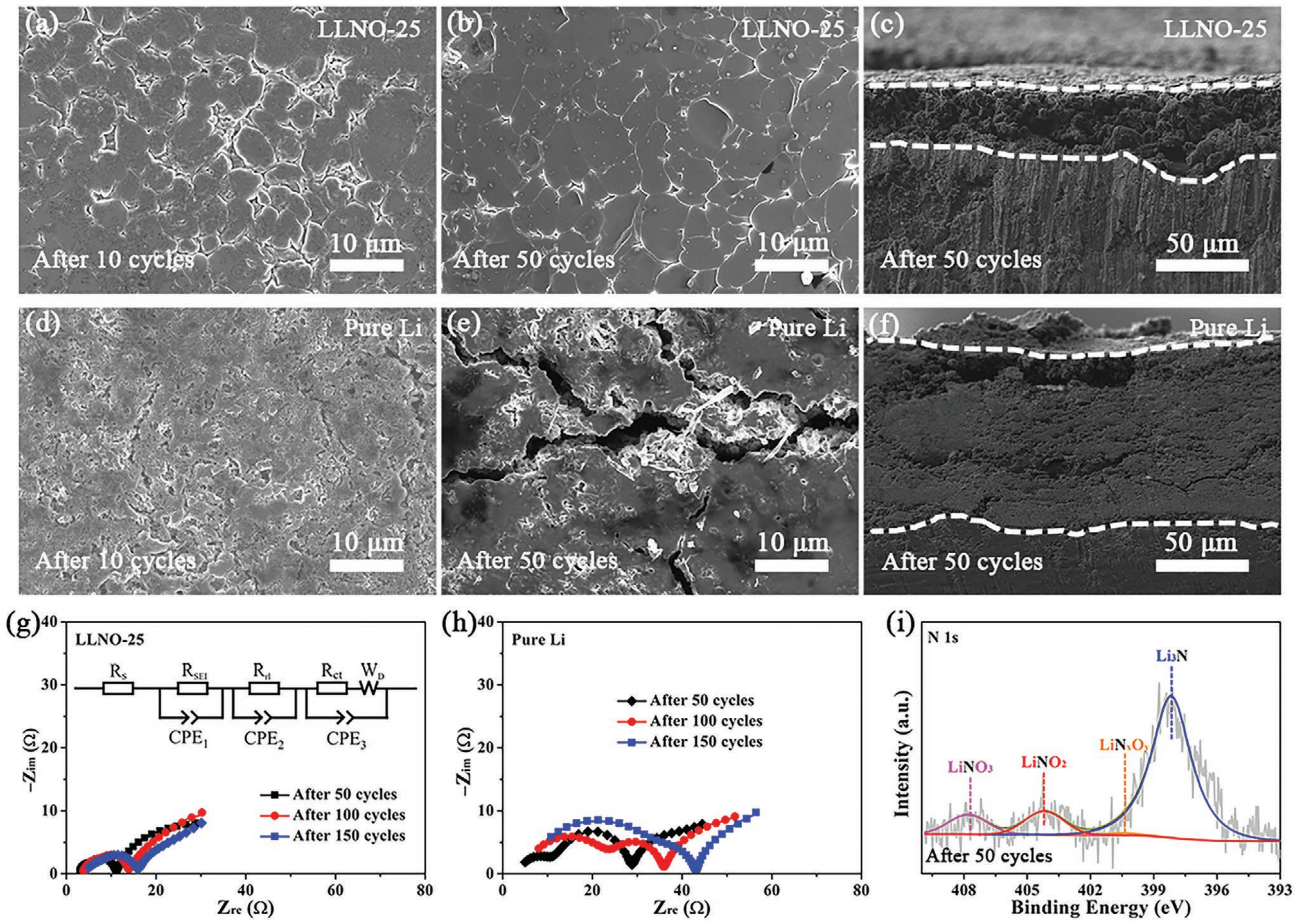

Figure 3. Structure evaluation of the pure Li and LLNO-25 composite electrodes on cycling by testing LLNO-25||LLNO-25 and Li||Li symmetric cells at 1 mA cm^{-2} and 1 mA h cm^{-2}. a) Top-view SEM image of a LLNO-25 electrode after 10 cycles. b) Top-view and c) cross-sectional SEM images of a LLNO-25 electrode after 50 cycles. d) Top-view SEM image of a pure Li electrode after 10 cycles. e) Top-view and f) cross-sectional SEM images of a pure Li electrode after 50 cycles. Nyquist plots of g) the LLNO-25 composite and h) pure Li electrodes after 50, 100, and 150 cycles. The inset shows the corresponding equivalent circuit model, where R_s, R_{SEI}, R_{rl}, and R_{ct} represent the solution, SEI film, reaction layer, and charge transfer resistances, respectively. i) High-resolution N 1s XPS spectra of a LLNO-25 electrode after 50 cycles (20 min of Ar-ion etching).

that of the pure metallic Li in each tested cycle, the latter of which increases quickly with the increase of cycle number. The values of R_{SEI} (resistance from SEI) are 2.08 and 6.79 Ω for the LLNO-25 electrode after 50 and 150 cycles, respectively. In contrast, the corresponding values are 8.32 and 32.91 Ω for the pure Li metal electrodes (Table S2, Supporting Information). The rapid increase of R_{SEI} for pure Li electrode on cycling can be ascribed to the fast accumulation of SEI film due to its repetitive breaking-rearranging during cycling. The LLNO-25 electrode displays stable R_{rl} (impedance from the reaction layer of electrodes) with negligible change for the tested cycles (50th cycle, 100th cycle, and 150th cycle), indicating that $LiNO_3$ in the LLNO-25 electrode can effectively reinforce the SEI and stabilize the Li plating. On the other hand, the R_{rl} for the pure Li metal electrode decreases from 17.25 Ω for the 50th cycle to 6.16 Ω for the 100th cycle probably due to the pulverization of reaction layer which creates increased contact interface between the active electrode and electrolyte. To understand the positive effect of $LiNO_3$ in improving the electrochemical performance of LLNO electrode, XPS analysis was conducted for the LLNO-25 electrode after 50 cycles. Ar-ion etching (20 min) was carried out before the collection of XPS information. Figure 3i shows the high-resolution N1s XPS spectrum of the cycled LLNO-25 electrode. The N 1s core level region presents three obvious peaks at 398.2, 404.2, and 407.8 eV, which can be attributed the signals of Li_3N, $LiNO_2$, and $LiNO_3$, respectively.[24,30–32] Compared with the pristine LLNO-25 electrode (Figure 2d), the relative intensity of the Li_3N peak increases significantly and other two peaks display relatively lower peak intensity suggesting the further reduction of $LiNO_3$ and generation of $LiNO_3$ derivatives over cycling. The strong XPS characteristic peaks of Li_2O are detected in the Li 1s (54.25 eV) and O 1s (528.0 eV) spectra (Figure S20, Supporting Information), which verifies the existence of Li_2O.[24,25,30] Li_3N, LiN_xO_y and Li_2O help to construct a stable Li metal electrode with stable SEI, while Li_3N and LiN_xO_y can enhance the conductivity of the electrode due to their high Li^+ conductivity.[28] Also, Li_2O can improve the mechanical strength of SEI, and thus enable good stability during the cycling.[41] The $LiNO_3$ and formation of its derivatives enable much more stable SEI and higher electrochemical

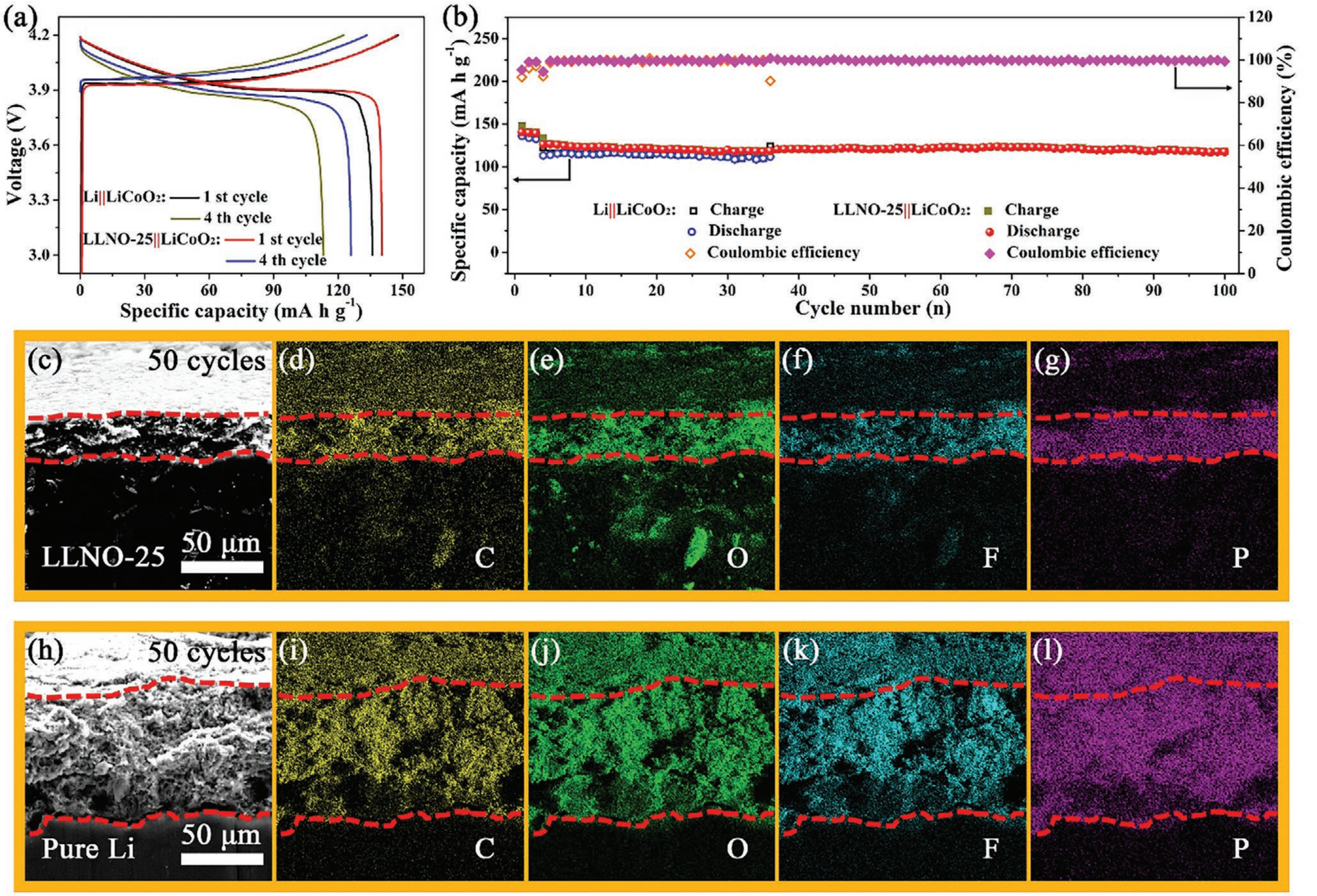

Figure 4. Electrochemical performances of the pure Li anode and LLNO-25 composite anode coupled with high-loading commercial $LiCoO_2$ cathode (≈20 mg cm^{-2}) at a current density of 0.1 C (the first three cycles) and 0.5 C (the following cycles). a) Voltage profiles of the LLNO-25|| $LiCoO_2$ and $LiCoO_2$||Li cells and b) their corresponding cycling performance. c) Cross-sectional SEM image of a LLNO-25 composite anode after 50 cycles and d–g) the corresponding EDS mapping images. h) Cross-sectional SEM image of a pure Li anode after 50 cycles and i–l) the corresponding EDS mapping images.

reversibility of metallic Li in comparison to the pure Li, accompanied by lower consumption of liquid electrolyte and production of "dead Li".[29] In fact, the corrosion of pure metallic Li in carbonate-based electrolyte is very severe and causes fast battery degradation, which has been widely reported.[42,43] A Li metal full cell with a cathode with commercial-level areal capacity loading can only cycle for <50 cycles in carbonate-based electrolyte due to the exhaustion of electrolyte and formation of very thick SEI on the anode.[10,44]

To show the ability of LLNO electrode in suppressing the side reactions between electrolyte and metallic Li, electrochemical cycling evaluation was conducted under a lean electrolyte condition. For practical application, full cells in coin cell configuration were assembled by pairing the LLNO-25 anode (or pure Li anode) with commercial high-loading $LiCoO_2$ cathode (≈20 mg cm^{-2}, Figure S21, Supporting Information) using lean electrolyte volume of ≈12 µL. These cells were tested at 0.5 C (1 C = 140 mA g^{-1}) after three activation cycles at 0.1 C. As shown in **Figure 4**a, identical charge and discharge plateaus and similar specific capacities were achieved in both cells at the initial cycles, suggesting stable electrochemical behavior of the LLNO-25 electrode. Distinct increase in polarization was observed in voltage curves of the Li||$LiCoO_2$ cell with cycle increase (Figure 4a and Figure S22, Supporting Information), indicating the increase of impedance due to the consumption of electrolyte, companied by the increase of reaction layer. Significant difference was found, where the LLNO-25||$LiCoO_2$ cell maintained a stable cycling capacity and Li||$LiCoO_2$ cell failed after 37 cycles (Figure 4b and Figure S22, Supporting Information). These results suggest the significant role of $LiNO_3$ from the LLNO composite in extending the cycle life of batteries in harsh conditions. After 100 cycles, a high capacity retention of 93.1% for LLNO-25||$LiCoO_2$ cell is achieved (Figure 4b). The superior cycling stability of the batteries using LLNO-25 anode under lean electrolyte condition is ascribed to the presence of $LiNO_3$ and its derivatives in the composite electrode that enables a stable SEI and reduces the corrosion of metallic Li against carbonate-based electrolyte. To investigate the structures of the LLNO-25 and pure Li electrodes after cycling, LLNO-25||$LiCoO_2$ and Li||$LiCoO_2$ cells were assembled with ≈50 µL electrolyte and cycled at 0.5 C for 50 cycles (Figure S23, Supporting Information). The LLNO-25 electrode delivers a thin reaction layer (≈26 µm) after 50 charge/discharge cycles (Figure 4c-g), while the reaction layer of pure Li anode reaches about 82 µm

(Figure 4h-l), which are in agreement with results of symmetric cells. The strong signals of C, O, F, and P were observed in the corresponding EDS elemental mapping images (Figure 4d-g for the LLNO-25 and Figure 4i-l for the pure Li), which arise from the decomposition and permeation of electrolyte into the porous reaction layer. This result indicates that the introduction of $LiNO_3$ can stabilize the active Li/electrolyte interface and suppress the consumption of active Li and electrolyte. Figure S24, Supporting Information illustrates the failure mechanism of the pure Li and LLNO-25 composite anodes. For pure Li anode, the repeated uneven plating/stripping of mossy Li with high surface area leads to the continuous breaking and re-forming of SEI during cycling and a loose electrode structure. Also, this process continuously consumes active Li and electrolyte, and finally results in the fast failure of Li electrode. As comparison, the plated Li deposits with stable SEI can reduce the consumption of active Li and electrolyte, resulting in prolonged cycle life of the LLNO-25 composite electrode. To further evaluate the chemical stability of the LLZO-25 composite and pure Li against electrolyte, SEM was employed to investigate the thickness of the corrosion/passivation layers after immersing the electrodes in electrolyte for 150 h (Figure S25, Supporting Information). As shown in Figure S26, Supporting Information, the passivation layer of the pure Li foil is about three times the thickness of the LLZO-25 composite foil (≈28 µm for pure Li foil and ≈9 µm for LLZO-25 composite foil), again verifying that the uniform introduction of $LiNO_3$ in the bulk of metallic Li improves the chemical stability of metallic Li electrode against carbonate-based solvents.

3. Conclusion

In summary, we fabricated a "salt-in-metal" metallic Li based composite anode by introducing $LiNO_3$ additive into the bulk of metallic Li using a facile mechanical kneading approach, which helps to construct a stable SEI and enable reversible battery cycling in a lean carbonate electrolyte condition. Conceptually, the introduction of $LiNO_3$ into metallic Li electrode provides new insights for addressing the challenge of electrolyte additives with low solubility in commercial carbonate electrolytes. Technically, cold rolling approach is facile, safe and economical. In the as-fabricated LLNO electrode, $LiNO_3$ was embedded in the entire metallic Li electrode. The $LiNO_3$ derived derivatives work as functional component in the SEI, helping to increase the ionic conductivity, decrease the nucleation energy barrier, and regulate the uniform plating/stripping of metallic Li. Moreover, the coexistence of $LiNO_3$ and its derivatives can reinforce the initial SEI and in-situ repair the damaged SEI resulting from Li stripping/plating, hence enabling long-term cycle life. Li deposits with uniform morphology and large size are observed for the cycled LLNO-25 composite. $LiCoO_2$||LLNO-25 full cell with high cathode loading using lean electrolyte volume of ≈12 µL exhibits stable cycling and displays a high capacity retention of 93.1% after 100 cycles at 0.5 C. In contrast, fast capacity decay of the counterpart using pure Li anode is observed. Based on the facile synthesis and much improved electrochemical performance, we firmly believe that introduction of $LiNO_3$ into the bulk metallic Li via a mechanical kneading approach provides an alternative strategy to address the low solubility of additives in electrolyte and is promising for practical application in rechargeable Li metal batteries. Also, the concept of "salt-in-metal" can be extended to other electrolyte additives and alkali metal electrode systems.

4. Experimental Section

All experimental details are included in the Supporting Information.

Supporting Information

Supporting Information is available from the Wiley Online Library or from the author.

Acknowledgements

Y.S. acknowledges the financial support by and the National Natural Science Foundation of China (No. 52002136, 51802105), and the Innovation Fund of Wuhan National Laboratory for Optoelectronics of Huazhong University of Science and Technology. Z.C. thanks the China Postdoctoral Science Foundation (No. 2018M640694, 2020T130223). Z.W.S. acknowledges the support of the Singapore National Research Foundation (NRF-NRFF2017-04). The authors would like to thank the Analytical and Testing Center of Huazhong University of Science and Technology as well as the Center for Nanoscale Characterization and Devices of Wuhan National Laboratory for Optoelectronics for providing the facilities to conduct the characterization. L.F. would like to thanks the Mikrouna (www.mikrouna.com) and eceshi (www.eceshi.com) for supporting the material preparation and characterization, respectively. The authors also acknowledge Qingwu Huang and Zihe Chen for XPS analysis and TOC design, respectively.

Conflict of Interest

The authors declare no conflict of interest.

Data Availability Statement

Research data are not shared.

Keywords

$LiNO_3$, lithium metal anodes, mechanical kneading, salt-in-metal, solid electrolyte interphase

Received: December 9, 2020
Revised: February 2, 2021

---

[1] X. B. Cheng, R. Zhang, C. Z. Zhao, Q. Zhang, *Chem. Rev.* **2017**, *117*, 10403.
[2] X. Liang, Q. Pang, I. R. Kochetkov, M. S. Sempere, H. Huang, X. Sun, L. F. Nazar, *Nat. Energy* **2017**, *2*, 17119.
[3] Q. Li, S. Zhu, Y. Lu, *Adv. Funct. Mater.* **2017**, *27*, 1606422.
[4] H. Qiu, T. Tang, M. Asif, X. Huang, Y. Hou, *Adv. Funct. Mater.* **2019**, *29*, 1808468.

[5] D. Lin, Y. Liu, Y. Cui, *Nat. Nanotechnol.* **2017**, *12*, 194.

[6] L. Ren, A. Wang, X. Zhang, G. Li, X. Liu, J. Luo, *Adv. Energy Mater.* **2019**, *10*, 1902932.

[7] E. Peled, S. Menkin, *J. Electrochem. Soc.* **2017**, *164*, A1703.

[8] Y. Gao, Z. Yan, J. L. Gray, X. He, D. Wang, T. Chen, Q. Huang, Y. C. Li, H. Wang, S. H. Kim, T. E. Mallouk, D. Wang, *Nat. Mater.* **2019**, *18*, 384.

[9] J. Xiao, *Science* **2019**, *366*, 426.

[10] J. Liu, Z. Bao, Y. Cui, E. J. Dufek, J. B. Goodenough, P. Khalifah, Q. Li, B. Y. Liaw, P. Liu, A. Manthiram, Y. S. Meng, V. R. Subramanian, M. F. Toney, V. V. Viswanathan, M. S. Whittingham, J. Xiao, W. Xu, J. Yang, X.-Q. Yang, J.-G. Zhang, *Nat. Energy* **2019**, *4*, 180.

[11] C. Niu, H. Lee, S. Chen, Q. Li, J. Du, W. Xu, J.-G. Zhang, M. S. Whittingham, J. Xiao, J. Liu, *Nat. Energy* **2019**, *4*, 551.

[12] P. Zhai, L. Liu, X. Gu, T. Wang, Y. Gong, *Adv. Energy Mater.* **2020**, *10*, 2001257.

[13] Y. Zhao, G. Li, Y. Gao, D. Wang, Q. Huang, D. Wang, *ACS Energy Lett.* **2019**, *4*, 1271.

[14] S. Li, Q. Liu, J. Zhou, T. Pan, L. Gao, W. Zhang, L. Fan, Y. Lu, *Adv. Funct. Mater.* **2019**, *29*, 1808847.

[15] H. Liu, X.-B. Cheng, J.-Q. Huang, H. Yuan, Y. Lu, C. Yan, G.-L. Zhu, R. Xu, C.-Z. Zhao, L.-P. Hou, C. He, S. Kaskel, Q. Zhang, *ACS Energy Lett.* **2020**, *5*, 833.

[16] X. Shangguan, G. Xu, Z. Cui, Q. Wang, X. Du, K. Chen, S. Huang, G. Jia, F. Li, X. Wang, D. Lu, S. Dong, G. Cui, *Small* **2019**, *15*, 1900269.

[17] H. Zhang, G. G. Eshetu, X. Judez, C. Li, L. M. Rodriguez-Martinez, M. Armand, *Angew. Chem., Int. Ed.* **2018**, *57*, 15002.

[18] Z. A. Ghazi, Z. Sun, C. Sun, F. Qi, B. An, F. Li, H. M. Cheng, *Small* **2019**, *15*, 1900687.

[19] G. Yasin, M. Arif, T. Mehtab, X. Lu, D. Yu, N. Muhammad, M. T. Nazir, H. Song, *Energy Storage Mater.* **2020**, *25*, 644.

[20] X. Q. Zhang, T. Li, B. Q. Li, R. Zhang, P. Shi, C. Yan, J. Q. Huang, Q. Zhang, *Angew. Chem., Int. Ed.* **2020**, *59*, 3252.

[21] M. Liu, Z. Cheng, K. Qian, T. Verhallen, C. Wang, M. Wagemaker, *Chem. Mater.* **2019**, *31*, 4564.

[22] C. Yan, Y. X. Yao, X. Chen, X. B. Cheng, X. Q. Zhang, J. Q. Huang, Q. Zhang, *Angew. Chem., Int. Ed.* **2018**, *57*, 14055.

[23] X. Wang, H. Wang, M. Liu, W. Li, *Small* **2020**, *16*, 2000769.

[24] Y. Liu, D. Lin, Y. Li, G. Chen, A. Pei, O. Nix, Y. Li, Y. Cui, *Nat. Commun.* **2018**, *9*, 3656.

[25] W. Zhang, Q. Wu, J. Huang, L. Fan, Z. Shen, Y. He, Q. Feng, G. Zhu, Y. Lu, *Adv. Mater.* **2020**, *32*, 2001740.

[26] The Materials Project https://www.materialsproject.org (accessed: August 2020).

[27] X. Guan, A. Wang, S. Liu, G. Li, F. Liang, Y. W. Yang, X. Liu, J. Luo, *Small* **2018**, *14*, 1801423.

[28] Q. Shi, Y. Zhong, M. Wu, H. Wang, H. Wang, *Proc. Natl. Acad. Sci. USA* **2018**, *115*, 5676.

[29] W. Zhang, Z. Shen, S. Li, L. Fan, X. Wang, F. Chen, X. Zang, T. Wu, F. Ma, Y. Lu, *Adv. Funct. Mater.* **2020**, *30*, 2003800.

[30] N. A. Sahalie, A. A. Assegie, W.-N. Su, Z. T. Wondimkun, B. A. Jote, B. Thirumalraj, C.-J. Huang, Y.-W. Yang, B.-J. Hwang, *J. Power Sources* **2019**, *437*, 226912.

[31] W. Qi, L. Ben, H. Yu, Y. Zhan, W. Zhao, X. Huang, *J. Power Sources* **2019**, *424*, 150.

[32] C. C. Nguyen, B. L. Lucht, *J. Electrochem. Soc.* **2018**, *165*, A2154.

[33] X. Q. Zhang, X. Chen, X. B. Cheng, B. Q. Li, X. Shen, C. Yan, J. Q. Huang, Q. Zhang, *Angew. Chem., Int. Ed.* **2018**, *57*, 5301.

[34] Z. Wang, F. Qi, L. Yin, Y. Shi, C. Sun, B. An, H. M. Cheng, F. Li, *Adv. Energy Mater.* **2020**, *10*, 1903843.

[35] Y. Ouyang, Y. Guo, D. Li, Y. Wei, T. Zhai, H. Li, *ACS Appl. Mater. Interfaces* **2019**, *11*, 11360.

[36] Y. X. Yao, X. Q. Zhang, B. Q. Li, C. Yan, P. Y. Chen, J. Q. Huang, Q. Zhang, *InfoMat* **2020**, *2*, 379.

[37] Y. Lin, Z. Wen, C. Yang, P. Zhang, J. Zhao, *Electrochem. Commun.* **2019**, *108*, 106565.

[38] J. Meng, F. Chu, J. Hu, C. Li, *Adv. Funct. Mater.* **2019**, *29*, 1902220.

[39] Z. Tu, S. Choudhury, M. J. Zachman, S. Wei, K. Zhang, L. F. Kourkoutis, L. A. Archer, *Nat. Energy* **2018**, *3*, 310.

[40] Y. Liu, X. Qin, D. Zhou, H. Xia, S. Zhang, G. Chen, F. Kang, B. Li, *Energy Storage Mater* **2020**, *24*, 229.

[41] S. Li, W. Zhang, Q. Wu, L. Fan, X. Wang, X. Wang, Z. Shen, Y. He, Y. Lu, *Angew. Chem., Int. Ed.* **2020**, *59*, 14935.

[42] Y. Guo, H. Li, T. Zhai, *Adv. Mater.* **2017**, *29*, 1700007.

[43] A. Kolesnikov, M. Kolek, J. F. Dohmann, F. Horsthemke, M. Börner, P. Bieker, M. Winter, M. C. Stan, *Adv. Energy Mater.* **2020**, *10*, 2000017.

[44] D. Lu, Y. Shao, T. Lozano, W. D. Bennett, G. L. Graff, B. Polzin, J. Zhang, M. H. Engelhard, N. T. Saenz, W. A. Henderson, P. Bhattacharya, J. Liu, J. Xiao, *Adv. Energy Mater.* **2015**, *5*, 1400993.